

Detailed analysis of the Raman response of n -doped double-wall carbon nanotubesH. Rauf,¹ T. Pichler,¹ R. Pfeiffer,² F. Simon,^{2,*} H. Kuzmany,² and V. N. Popov³¹*IFW Dresden, P.O. Box 270116, D-01171 Dresden, Germany*²*Fakultät für Physik der Universität Wien, Strudlhofgasse 4, 1090 Wien, Austria*³*Faculty of Physics, University of Sofia, Sofia, Bulgaria*

(Received 21 August 2006; revised manuscript received 27 October 2006; published 12 December 2006)

We report on detailed studies of the n -type doping dependence of the Raman response of double-wall carbon nanotubes using potassium intercalation. The charge transfer is monitored by a shift of the G line. Upon doping the G line shifts to higher frequencies for the outer and to lower frequencies for the inner tubes. This is explained by different Coulomb interactions for the inner and outer tubes. The response of the radial breathing mode upon doping shows that a charge transfer from the dopant happens predominantly to the outer tubes at low doping. Charge transfer to the inner tubes occurs at higher doping levels. The previously observed cluster behavior of the inner tube RBM response allows a detailed analysis of the dependence of the inner tube doping from specific inner tube–outer tube configurations.

DOI: [10.1103/PhysRevB.74.235419](https://doi.org/10.1103/PhysRevB.74.235419)

PACS number(s): 78.30.Na, 78.66.Tr, 63.20.Dj, 78.67.Ch

I. INTRODUCTION

Double-wall carbon nanotubes (DWCNTs) are a member in the family of well-ordered carbon structures.^{1,2} Due to their formation from C_{60} peapods as precursor in the clean interior of single-wall carbon nanotubes (SWCNTs), the inner tubes are highly defect-free.³ As it has been demonstrated for other nanostructures,^{4,5} the electronic structure can be modified in a controlled way by doping with either electron donors or acceptors.

Resonant Raman spectroscopy is a powerful tool to monitor the electronic properties⁴ and their changes due to the interaction between transitions in the electronic density of states and the vibrational modes. The intensity of the Raman response increases dramatically if the excitation energy corresponds to a transition between Van Hove singularities (VHSs) in the electronic density of states or between excitons.⁶ Thus, by using different laser energies for excitation, particular transitions can be predominantly excited in order to achieve resonance for the nanotubes with corresponding diameter. For SWCNTs, the most important features in the Raman spectrum are the G line and the radial breathing mode (RBM). The G line derives from several strong tangential modes and can be found between 1500 and 1600 cm^{-1} . The RBM for conventional SWCNTs can be located in the low-frequency region around 200 cm^{-1} . For large diameter SWCNTs, both the transition energy and the RBM frequency scale roughly with the inverse diameter. For smaller SWCNT with diameters $d \lesssim 1$ nm curvature effects lead to discernible deviations from this relation⁷ which can be categorized in a family pattern⁸ where all SWCNTs with $(2n+m)=l$ form a family l . The SWCNT are further classified as semiconducting type I (SI) if $(2n+m) \bmod 3=1$ and semiconducting type II (SII) if $(2n+m) \bmod 3=2$. SWCNTs with $(2n+m) \bmod 3=0$ are metallic.

In DWCNTs the inner tubes give rise to additional RBMs. As the Raman shift of the RBM scales inversely proportional to the tube diameter, the RBMs of inner and outer tubes in DWCNTs are clearly distinguishable in the spectrum. The signal from the inner tubes also spreads over a wider spectral

range with unusual narrow linewidths³ and exhibits more lines than there are geometrically allowed inner tubes. This is ascribed to the fact that tubes with different diameters can act as outer tubes for one specific inner tube and that the diameter difference of inner and outer tube affects the inner tube RBM. This leads not only to the possibility to identify the response from nanotubes with distinct chirality pairs within the spectrum of these sharp RBM lines but also permits the assignment of the individual peaks from one inner tube cluster to a specific inner tube–outer tube combination.⁹

Intercalation with either electron donors (n -type doping) or acceptors (p -type doping) is a method to change the electronic properties in a controlled manner. According to the type of doping the Fermi level can be shifted upwards (n -type doping) or downwards (p -type doping). In the picture of a rigid band structure, it is most interesting to observe what happens if the Fermi level is shifted beyond VHSs thus resulting in the loss of optical transitions and Raman resonance. In a bulk sample, nanotubes form bundles where the tubes are packed in a hexagonal lattice bound by van der Waals forces. Intercalants such as potassium are predominantly located in the channels between the tubes.¹⁰

In this paper we present a detailed study of the potassium intercalation (n -type doping) of peapod grown DWCNTs investigated by transport and Raman spectroscopy. We examine the effect of doping on the G line as well as on the RBM. Upon doping the G line of the outer tubes shifts to higher frequencies and the G line of the inner tubes shifts to lower frequencies. A model is used to explain this different behavior through the Coulomb interactions in the unequal environments of the inner and outer tubes. The high-resolution response of the DWCNT (8,3) and (7,5) inner tubes exhibits multiple lines due to a dependence of the inner tube RBM on the outer tube, or more specifically, on the diameter difference between inner and outer tube. The analysis of the components of these clusters allows the detailed study of the doping dependence of specific inner tube–outer tube configurations where a complex behavior was found.

II. EXPERIMENTAL

The SWCNTs starting material was produced by arc-discharge, purified, and filtrated into mats of bucky paper as described elsewhere.¹¹ The tubes had a mean diameter of 1.45 nm and were subsequently filled with C₆₀ as described previously.¹² Subsequent annealing in order to form DWCNTs was performed at 1250 °C for 2 h in dynamic vacuum.

All Raman spectra were recorded at 25 K under high vacuum conditions with a Dilor triple monochromator spectrometer in 180° backscattering geometry. The samples were excited using the 676 nm (1.83 eV), 568 nm (2.18 eV), and 488 nm (2.54 eV) lines of an Ar/Kr laser. The Raman shift was calibrated with several spectral calibration lamps from L.O.T.-Oriol. All spectra of one excitation energy were measured with the same laser power and if not noted otherwise, the scaling factors given in the figures denote the scaling of the as-measured spectra.

The intercalation was performed *in situ* in a purpose-built cryostat in front of the spectrometer by exposing the tubes material to potassium vapor at a sample temperature of 500 K. After the exposure, an additional equilibration of at least 30 min was performed in order to increase the homogeneity of the sample. During cooling from the equilibration temperature to the measurement temperature, the resistance of the DWCNTs bucky paper was measured with the four-point method.

III. RESULTS

The most important effect for resonant Raman studies of doped carbon nanotube systems is the loss of resonance due to a filling or depletion of the VHSs by *n*-type or *p*-type doping, respectively. The use of different laser energies allows to study different transitions of tubes with a specific chirality (*m, n*) which can be identified using the well-known Kataura plot.^{7,13}

Within a simplified band model¹⁴ (i.e., ignoring excitons and interference effects discussed in Refs. 15 and 16), the Stokes Raman intensity *I* of a mode with phonon energy E_{ph} varies with the laser excitation energy E_L as

$$I(E_L) \propto \frac{|J_{ii}|^2}{|(E_L - E_{ii} - i\Gamma)(E_L - E_{\text{ph}} - E_{ii} - i\Gamma)|^2}, \quad (1)$$

where E_{ii} is the transition energy, J_{ii} determines the maximum intensity, and Γ is a damping parameter which describes the relaxation of the optically excited state. Since all the tubes discussed in the following exhibit approximately the same values for $|J_{ii}|$, the relative intensities of the Raman peaks are given by the (*n, m*) population and the resonance conditions. For $E_{\text{ph}} < 2\Gamma$ —typical for the RBM—the intensity profile has only one maximum at $E_L = E_{ii} + E_{\text{ph}}/2$. If $E_{\text{ph}} \gg 2\Gamma$ —typical for the G mode—there are two intensity maximums at $E_L \gtrsim E_{ii}$ (“incoming resonance”) and at $E_L \lesssim E_{ii} + E_{\text{ph}}$ (“outgoing resonance”).

With a mean diameter of 1.45 nm for the outer tubes the diameters of the inner tubes are expected to be in the range of 0.65–0.85 nm.¹¹ According to the DWCNT Raman map

in Ref. 9, the 2.54 eV (488 nm) excitation leads to a Raman resonance with the E_{33}^S and E_{44}^S transitions of the outer tubes while almost no inner tubes are in resonance. For a 2.18 eV (568 nm) excitation the outer tubes resonate with the E_{33}^S transition and some inner tubes of family $2m+n=24$ resonating with E_{11}^M and of families 16, 17, and 20 resonating with E_{22}^S can be seen in the spectra. Finally, exciting the DWCNT sample with 1.83 eV (676 nm) the outer tubes of families 30 and 33 resonate with the E_{11}^M transition and the inner tubes—mainly of family 19—resonate with the E_{22}^S transition.

A. Pristine SWCNTs and DWCNTs

1. Tangential mode region

The tangential G line of SWCNTs consists of six modes ($2A_1 + 2E_1 + 2E_2$) for chiral tubes and of three modes ($A_{1g} + E_{1g} + E_{2g}$) for achiral tubes, where most of the intensity comes from the A_1 modes.^{14,17} These modes are approximately longitudinal (LO) or transverse (TO) with respect to the tube axis. Depending on the diameter distribution in the SWCNTs sample, one usually observes in the experiments a strong G^+ subband around 1594 cm^{-1} and a smaller G^- subband split into two components around 1570 and 1554 cm^{-1} (see upper part of Fig. 1). The frequencies of all modes in the G subbands for (mainly achiral) tubes in the diameter range 0.5–1.6 nm were first calculated using density functional theory (DFT).¹⁸ Recent symmetry-adapted nonorthogonal tight-binding (NTB) calculations support and extend the DFT results to smaller and larger diameters (0.4–2.4 nm) and all geometrically allowed tubes in this diameter range.¹⁹

The G^+ peak is mainly the $A_1^{\text{LO}}(S)$ mode of semiconducting tubes.¹⁴ For typical SWCNTs samples with a diameter distribution centered around 1.45 nm the intensity of the G^+ peak decreases when shifting the excitation from blue to red, since the number of semiconducting tubes close to resonance decreases strongly. NTB calculations¹⁹ showed that for tubes with diameters $D \geq 1$ nm the frequency of the $A_1^{\text{LO}}(S)$ mode is about 1592 cm^{-1} almost independent of diameter and chirality. For thinner tubes the frequency decreases with decreasing diameter. After scaling with a factor of 0.9000, the NTB results match very well with the DFT calculated frequencies in Ref. 18 except that on average the NTB frequencies are about 7.0 cm^{-1} below the DFT values.

The higher frequency component of the G^- peak is mainly the $A_1^{\text{TO}}(M, S)$ mode of metallic and semiconducting tubes while the lower frequency component is mainly the $A_1^{\text{LO}}(M)$ mode of metallic tubes.¹⁴ Both components shift to lower frequencies with decreasing tube diameter. The NTB results for the $A_1^{\text{TO}}(M, S)$ mode again compare very well with the DFT results, with an average downshift of about 7.5 cm^{-1} . However, for the $A_1^{\text{LO}}(M)$ component, the discrepancy is about 27 cm^{-1} on the average. This large deviation stems from the incomplete Coulomb screening in the NTB model.

In Fig. 1 the Raman spectra after the first (light) doping step of SWCNTs and DWCNTs are depicted for the three laser excitations studied. This facilitates the identification of the inner tubes contribution since, while the spectra remain qualitatively the same (see Fig. 5), the response from the

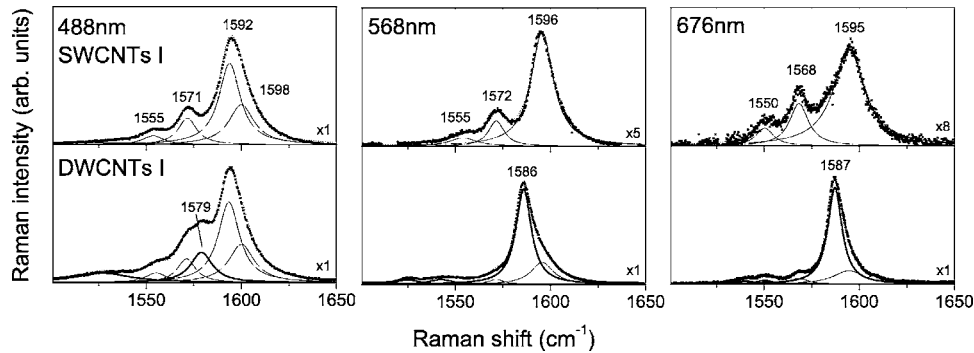


FIG. 1. G-line spectra of lightly doped SWCNTs (upper panel, black squares) and DWCNTs (lower panel, black squares) for three different laser energies as indicated in the figures. The numbers indicate the peak positions as obtained from the fit. The spectra are fitted with Lorentzian line shapes (solid lines for the components and dotted lines for the sums). The components which are assigned to the inner tubes in the DWCNTs fit are marked by thick black lines. The multipliers in the SWCNT spectra indicate the factor by which the spectra are upscaled as compared to their contribution to the corresponding DWCNT spectra.

outer tubes decreased already significantly. This is especially important for the 488 nm excitation, where the overall Raman response mainly comes from the outer tubes, making an identification of the inner tube contribution difficult in the pristine state.

The SWCNTs spectra were fitted with four (488 nm) and three (568 and 676 nm) Lorentzians, respectively, to match the G^+ and the two G^- components. The extra peak around 1598 cm^{-1} in the 488 nm spectra originates probably from the $E_1^{\text{TO}}(\text{M},\text{S})$ modes.¹⁹ The fit for this excitation was carried out in close analogy to that in Ref. 20, where a $^{12}\text{C} \rightarrow ^{13}\text{C}$ isotope substitution was used to identify the inner tube contribution.

In order to identify the inner tubes contribution in the spectra of the DWCNTs, these spectra were fitted with Lorentzians where the contribution of the outer tubes is given by peaks with the same positions, widths, and relative intensities as in the SWCNTs spectra. A very good fit of the complete DWCNTs spectra could be achieved in this way for all three excitations with the addition of just one strong and one or two weak lines representing the inner tubes response. The main inner tubes peak was found at 1579 cm^{-1} (488 nm), 1586 cm^{-1} (568 nm), and 1587 cm^{-1} (676 nm), respectively. This is again in very good agreement with previous results, where additional inner tubes contributions of a DWCNTs sample compared to a SWCNTs sample at various laser excitations were found at 1587 cm^{-1} (647 nm),²¹ 1581 cm^{-1} (1064 nm), and 1580 cm^{-1} (514 nm).²² For all excitations the high frequency inner tubes peak lies about 10 cm^{-1} below the G^+ peak of the outer tubes. The second contribution from the inner tubes lies at Raman shifts of 1525 cm^{-1} (488 and 568 nm) and 1540 cm^{-1} (676 nm), respectively, with varying width and spectral weight in each case.

In the following, we will discuss only the strong peak of the inner tubes which we assign to the $A_1^{\text{LO}}(\text{S})$ component. Although the metallic tubes close to resonance with the used excitation energies have J_{ii} values whose magnitudes are comparable to that of the semiconducting tubes, most of the intensity is lost due to destructive interference effects.¹⁴ Additionally, the J_{ii} values for most tubes contributing to the

$A_1^{\text{TO}}(\text{S})$ component are much smaller than for the $A_1^{\text{LO}}(\text{S})$ component.¹⁴ Therefore, the $A_1^{\text{LO}}(\text{M})$ and $A_1^{\text{TO}}(\text{M},\text{S})$ peaks are very weak (especially for the inner tubes).

Judging from the Raman map in Ref. 9, for the 488 nm excitation there are only two semiconducting inner tubes close to outgoing resonance with their E_{22}^{S} transitions. These are the (5,4) tube in family 14 and the (7,3) tube in family 17. The NTB calculated $A_1^{\text{LO}}(\text{S})$ frequencies of these tubes are 1583.4 and 1583.3 cm^{-1} , respectively. Both frequencies are in very good agreement with the measured frequency of the inner tubes peak at 1579 cm^{-1} . This peak is of course much smaller than the corresponding outer tubes peak, where many different tubes contribute with incoming and outgoing resonances with their E_{33}^{S} and E_{44}^{S} transitions.

For the 568 nm excitation the (10,0), (9,2), and the (6,5) inner tubes are close to incoming resonance and the (6,4), (8,4), and (11,1) inner tubes are close to outgoing resonance with E_{22}^{S} . The average calculated $A_1^{\text{LO}}(\text{S})$ frequency of these tubes is $1587(2)\text{ cm}^{-1}$, which compares well with the peak at 1586 cm^{-1} .

For the 676 nm excitation the (8,3), (7,5), (7,6), (9,5), and (7,2) inner tubes are close to incoming resonance and the (8,7), (8,6), (9,4), (10,2), (11,0), and (9,1) inner tubes are close to outgoing resonance. The average calculated $A_1^{\text{LO}}(\text{S})$ frequency of these tubes is $1589(5)\text{ cm}^{-1}$, which is again in very good agreement with the peak at 1587 cm^{-1} . For this excitation almost no outer semiconducting tubes are close to resonance and thus the G^+ peak of the outer tubes is very weak.

We thus have unambiguously separated the DWCNTs spectra into contributions from the inner and outer tubes. This allows to examine the respective behavior upon doping of the sample.

2. Radial breathing mode region

We now investigate the Raman response in the radial breathing mode region between 125 and 375 cm^{-1} . The results for the 568 and the 676 nm excitations are depicted in Fig. 2. In the pristine state the response from the outer and inner tubes can be clearly distinguished. For the 568 nm excitation, the outer tubes signal consists of a broad feature

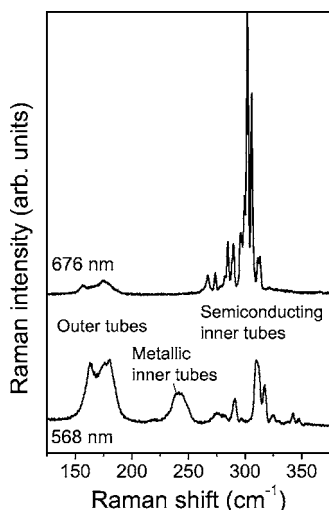


FIG. 2. Radial breathing mode region of pristine DWCNTs excited with 676 nm (upper curve) and 568 nm (lower curve) laser wavelength.

around 175 cm^{-1} . The main response from the inner tubes is spread over the range between 225 and 360 cm^{-1} and has a clearly visible fine structure. The broad peak around 250 cm^{-1} originates from metallic inner tubes of family 24, the peaks between about 275 and 305 cm^{-1} arise from semiconducting inner tubes of family 20, and between about 305 and 335 cm^{-1} and between 335 and 370 cm^{-1} one can observe the clusters of the (6,5) and (6,4) inner tubes of families 19 and 16, respectively.⁹ Upon 676 nm excitation, the outer tubes response is spread between 150 and 190 cm^{-1} and the inner tubes contribution exhibits a fine structure between 250 and 330 cm^{-1} originating mainly from the (7,5) and (8,3) semiconducting inner tubes of family 19. Upon 568 nm excitation the signal intensity of outer and inner tubes is comparable while the inner tubes signal clearly dominates the 676 nm response.

Additional information on the properties of DWCNTs can be obtained from the high-resolution spectrum of the inner tube response. In the spectrum, depicted in Fig. 3, several narrow and well-separated peaks can be identified. As demonstrated in Ref. 9, the RBM Raman response of the inner tubes exhibits more peaks than there are geometrically possible tubes. These peaks are grouped into clusters with similar resonance energy. It was concluded that each cluster represents one particular inner tube inside various different outer tubes and each member of a cluster represents a well defined inner/outer tube pair. The higher the frequency of a peak in a cluster the smaller the diameter-difference between inner and outer tube. This conclusion was supported by calculations taking into account the diameter-dependent interaction between inner and outer tubes. This model successfully described the fine structure of a (6,4) inner tube.⁹ We now use this model to analyze the fine structure in the high-resolution spectrum of the inner tubes region excited with the 676 nm laser. The spectrum of the pristine DWCNTs in the inner tube range is depicted in Fig. 3 together with the calculated peak positions for the (7,5) and (8,3) tubes of family 19.²³ For the 676 nm (1.83 eV) excitation the (8,3) tube is

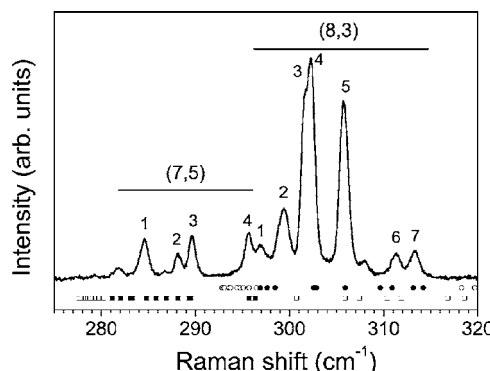


FIG. 3. High resolution spectrum of the undoped inner tubes region excited with 676 nm. The symbols represent calculated line positions for the inner tubes RBM depending on the outer tubes (solid squares for the (7,5) and solid circles for the (8,3) inner tubes, respectively).²³ Open symbols are for inner outer tube pairs which were not taken into account due to their very large/small diameter differences. The numbers indicate peaks used for the further evaluation.

very close to resonance. Therefore, slight changes in the transition energy will have only a minor influence on line intensity. In contrast, the (7,5) tube has its resonance at a noticeable higher energy. Therefore, the corresponding cluster appears weaker but even small changes in transition energy may lead to a change in line intensity. The (9,1) inner tube which also belongs to family 19 has its resonance around 1.7 eV and cannot be observed with a 1.83 eV excitation.^{9,23}

Fortunately, the clusters of the (7,5) and (8,3) inner tubes have only a small overlap region ($\approx 294\text{--}298\text{ cm}^{-1}$). Hence, the assignment of the individual peaks to either the (7,5) or the (8,3) cluster is straightforward especially for the first three numbered peaks of the (7,5) cluster and the last five numbered peaks of the (8,3) cluster (see Fig. 3). Since for family 19 the calculated RBM frequencies of specific inner tubes inside different outer tubes lie very close some peaks consist of two (or more) possible inner/outer tube combinations. This makes a meaningful assignment for the peaks of the (7,5) inner impossible. For the (8,3) inner tube peak 3 is most likely (8,3)@(15,6), peak 4 is likely (8,3)@(17,3), and peak 5 is probably (8,3)@(14,1). This means that peak 3 is a SI/M, peak 4 is a SI/SI, and peak 5 is a SI/SII inner/outer tube combination. This assignment later allows us to investigate the charge transfer to the inner tubes in detail by taking into account the variation of the diameter difference between inner and outer tubes.

B. Doping behavior of DWCNTs

1. Resistance

The resistance of the DWCNTs bucky paper is depicted in Fig. 4 as a function of temperature for all doping stages. After each doping step, it was measured over the whole temperature range starting at the equilibration temperature of ca. 500 K to the measuring temperature of 25 K. The doping steps are labeled in the figure with Roman numerals where 0

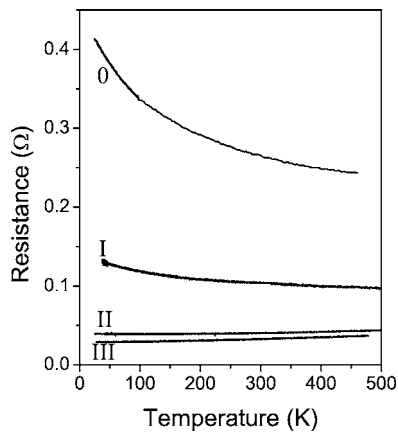


FIG. 4. Resistance of the DWCNTs bucky paper upon the different doping steps. The Roman numerals indicate the different doping steps as used in the following.

indicates the pristine state and III the highest doping step. Between the pristine state and the highest doping step, the room-temperature resistance of the sample decreases by about one order of magnitude as equally observed in previous doping experiments on SWCNTs.^{24–26} In the pristine state and in doping step I the sample resistance decreases with increasing temperature. This was observed in a similar way for SWCNTs in Refs. 26 and 27 and can be explained with hopping-type conductivity. Upon further doping—in steps II and III—the qualitative behavior changes: The resistance of the sample now increases with increasing temperature which indicates a more metallic behavior of the DWCNTs bucky paper similar to what was previously observed on K-doped C₆₀ peapods.⁵ In neither of the doping steps we observe a crossover of the temperature-dependent resistance from a negative slope to a positive slope which was seen in experiments of pristine²⁸ as well as Cs- and K-doped²⁶ SWCNTs.

2. Tangential mode region

The doping dependence of the DWCNT G line is depicted in Fig. 5 for all three laser excitations for the pristine case

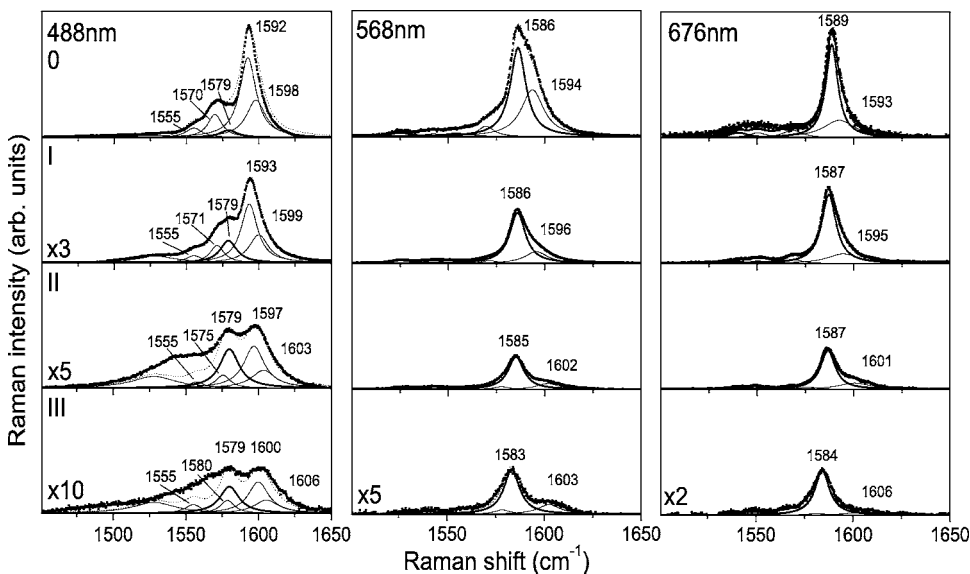


FIG. 5. Raman spectra of DWCNTs in the tangential mode region for the three different laser excitations (as indicated in the figures) at the different doping levels with increasing doping from top to bottom. The top spectra are the pristine DWCNTs. Squares represent the measured spectra and black lines represent the Lorentzian components of the fit. The sum of the Lorentzians, the overall fit result is given by dotted lines. The contribution from the inner tubes is highlighted as a thick curve. The numbers indicate the respective peak positions of the fitted curve.

and three doping steps with increasing doping from top to bottom. The spectra are fitted with Lorentzian line shapes according to the assignment taken from Fig. 1. The inner tubes contributions are highlighted with thick lines.

Upon doping the intensity of the outer tubes signal drops rapidly. This can be observed for all three excitation energies. Already at the first doping step the intensity decreased by roughly a factor of 3 to 4 indicating a loss of resonance due to a filling of the corresponding VHSs. On the other hand, the signal from the inner tubes is hardly decreased. Upon increased doping also the inner tubes signal decreases but still at a smaller rate than that of the outer tubes. More detail about this behavior will be discussed upon the investigation of the RBM region.

Another interesting influence of the doping on the Raman spectra concerns the peak positions of the different contributions from the outer and the inner tubes. They are derived from the fits of the spectra for the different doping steps. Constant relative intensities and relative peak positions were maintained in each of the two sets of fit components, those for the inner tubes and those for the outer tubes. All the spectra from the different doping levels and excitation wavelengths could be nicely fitted under these conditions (except for the two highest doping levels upon 488 nm excitation). The behavior is qualitatively the same for all three laser excitations and is summarized in Fig. 6. The components representing the outer tubes shift continuously to higher frequencies with increasing doping. The maximum shift depends on the respective excitation with values of 8 cm⁻¹ (488 nm), 9 cm⁻¹ (568 nm), and 13 cm⁻¹ (676 nm). On the other hand, the inner tubes components do not exhibit such behavior. Instead, the line position shows no shift in the case of the 488 nm excitation and exhibits small downshifts of 3 cm⁻¹ and 5 cm⁻¹ for the 568 and 676 nm excitations, respectively.

Sumanasekera *et al.* derived a relation between charge transfer and the G-line shift from electrochemical *p*-doping of SWCNT.²⁹ They obtained an upshift of the G line of 320 cm⁻¹ per hole per C atom. Assuming electron-hole symmetry, this corresponds to a charge transfer of approximately

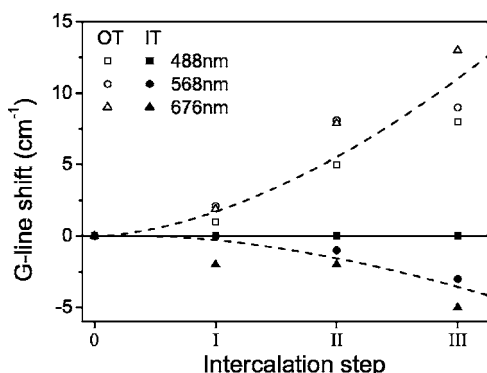


FIG. 6. Shift of the G line upon doping of outer (OT) and inner tubes (IT), respectively, as measured with different excitation energies. The shift of the outer tubes is given by open symbols and that of the inner tubes by solid symbols. The dashed lines are guides for the eye. The top axis shows the estimated charge transfer using the equation derived in Ref. 29.

0.3 electrons per carbon atom, i.e., a C/K ratio of ≈ 30 for the highest doping step depicted in Fig. 6. This analysis is complicated by the noncontinuous doping dependence as it was observed upon *n*-doping of SWCNT.^{25,30}

3. Radial breathing mode region

We now turn to the results of the influence of doping on the RBM response as they are depicted in Fig. 7. Upon doping the behavior is qualitatively the same for both excitation energies: In the first doping step (I) the response from the outer tubes decreases significantly whereas the inner tubes response is hardly changed. This is similar to the observation from the G line that the doping only affects the outer tubes at the beginning of doping and is in agreement with observations on the *p*-type doping of DWCNTs.²² However, in the 568 nm spectra it should be noted that the broad peak around 250 cm^{-1} from metallic inner tubes of family 24 decreases

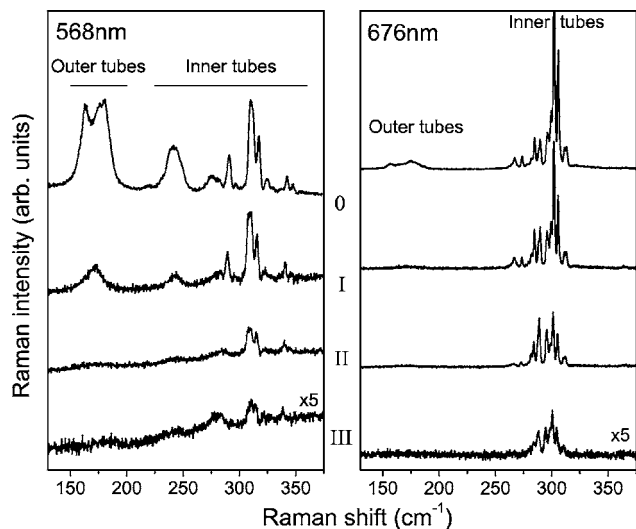


FIG. 7. Radial breathing mode region of the DWCNTs for the different doping steps excited with 568 and 676 nm laser wavelength.

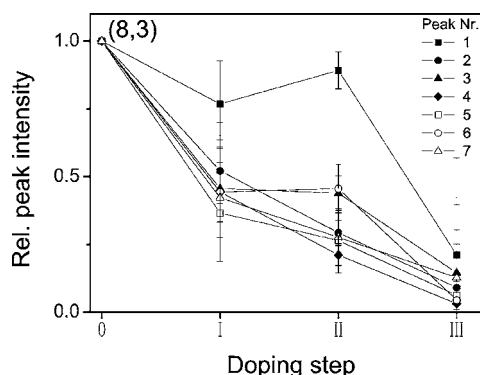


FIG. 8. Intensities of the peaks of the (8,3) cluster after the various doping steps relative to the undoped intensities as measured with a 676 nm excitation. The arrow next to the legend denotes the direction of decreasing diameter difference between inner tube and outer tube.

similar to the outer tubes response. At doping step II the outer tubes response has nearly vanished and the signal of the semiconducting inner tubes starts to decrease. With further doping (step III) the inner tubes signal continues to decrease but the fine structure is still present.

The assignment of the peaks of the inner tubes of the pristine DWCNTs can now be used to investigate to what extent the diameter difference between inner and outer tubes influences the charge transfer to the inner tubes. This should work particularly well for the (8,3) tubes since in this case a rather large number of inner/outer tube pairs can be observed. We fitted the 676 nm high-resolution spectra from the different doping steps (not shown) with Voigtians whose Gaussian part was determined by the spectrometer response function. From the fit we obtain the relative peak intensities compared to the pristine state, i.e., the change in intensity for each single peak we assigned previously. The results for the (8,3) and (7,5) inner tubes are plotted in Figs. 8 and 9, respectively. The individual peaks of each cluster are numbered according to Fig. 3 and the lower the number the larger the diameter difference between inner and outer tube.

In the (8,3) cluster the intensities of the peaks 2–7 drop to between 52 and 37% of their pristine values after doping step

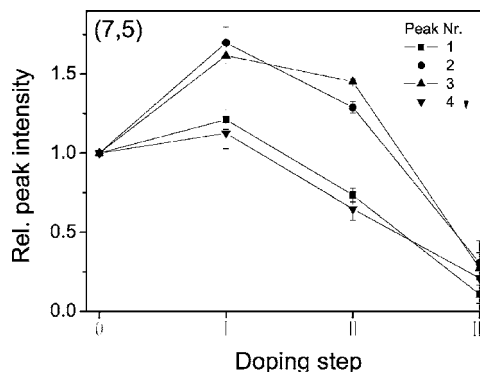


FIG. 9. Intensities of the peaks of the (7,5) cluster after the various doping steps relative to the undoped intensities as measured with a 676 nm excitation. The arrow next to the legend denotes the direction of decreasing diameter difference between inner tube and outer tube.

I. Interestingly, in addition to this strong decrease common for all these peaks, some details in the exact amounts are noticeable. The peaks where the distance between inner and outer tube is smaller (peaks 5–7) appear to decrease faster than those with a larger diameter difference (peaks 2–4). On further doping the intensities decrease similar for all peaks. The only exception to the described behavior is peak 1 which behaves very similar to the peaks of the (7,5) cluster. Since this peak is in the overlap region of the (7,5) and (8,3) clusters it might well have a large (7,5) contribution.

The general behavior of the peaks of the (7,5) cluster (Fig. 9) is that they increase (slightly) in intensity after the first doping step (I) before they start to decrease upon further doping (II and III). This behavior is best seen for peaks 2 and 3 and less expressed for peaks 1 and 4. Apart from this difference all inner/outer tube pairs behave similarly.

IV. DISCUSSION

The temperature-dependent resistance measurements exhibited an overall decrease in resistance of the DWCNT bucky paper by approximately one order of magnitude upon doping as well as a change in the slope of the temperature dependence from an increasing resistance with decreasing temperature for the pristine state and doping step I to a decreasing resistance with decreasing temperature for the two highest doping steps, II and III. This is explained by a more metallic behavior of the DWCNT bucky paper upon doping.³¹

For both the G line and the RBM response, the respective contributions of the inner and outer tubes of the DWCNTs to the overall response were identified and their behavior upon doping was analyzed. In both cases we could observe that already at the first doping step the outer tubes signal strongly decreases while the inner tube response is hardly affected. This leads—in agreement with previous studies for DWCNTs²² and C₆₀ peapods^{32,33}—to the conclusion that the charge from the potassium donor is predominantly transferred to the outer tubes in DWCNTs which leads to a filling of those VHSs in the conduction band which are responsible for the Raman resonance. However, charge transfer to the inner component starts earlier to the inner tubes in DWCNT than to C₆₀ in peapods.³⁴

The shift of the G line upon doping is controversial discussed in the literature. In graphite intercalation compounds (GICs) the shift depends on the type of intercalant. Upon *p*-type doping, the G mode hardens, and it softens upon *n*-type doping.³⁵ This behavior is explained by a contraction (expansion) of the C-C bonds in case of *p*-type (*n*-type) doping. For SWCNTs the behavior is expected to be similar. In Ref. 4 an upshift of the G line was indeed observed upon *p*-type doping of SWCNTs. For DWCNTs *p*-type doping, the G line was separated into contributions from the inner and outer tubes and the outer tubes component was found to shift upwards upon doping while the inner tubes component stayed at its original position.^{22,36} For *n*-type doping of SWCNTs from the vapor phase a behavior similar to our experiments, a nonmonotonic shift of the G line, was observed.^{25,30} For low doping the G line tends to upshift and

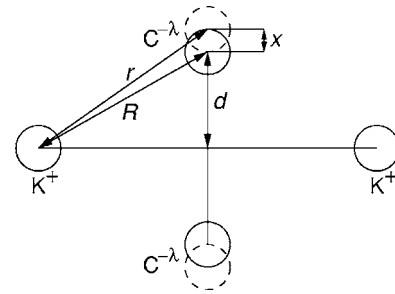


FIG. 10. Schematic representation of the model used for the G-line shift (see text). For simplicity a symmetric arrangement of ions is assumed.

then downshifts upon further doping. For Rb-doping this was explained by structural effects.²⁵ Upon Cs-doping anomalous behavior of the C-C bond length was stated.³⁰ The doping experiments at hand exhibit a continuous upshift of the outer tube G-line components while the main inner tube G-line component shifts down, although to a lesser extent.

In order to explain the origin of this unusual shift of the outer tubes G line, we suggest a simple model where the “G-line” frequency of a hypothetical C-C molecule is calculated as a function of charge transfer. The frequency shift is explained by the additional Coulomb interaction between the negatively charged carbon ions and between the carbon and potassium ions. A sketch of our model is shown in Fig. 10. The two carbon atoms have the equilibrium distance $2d = 0.14$ nm. In order to obtain the equation of motion we assumed that the unperturbed (undoped) system is a linear harmonic oscillator with the potential energy

$$U_0 = m\omega_0^2 x^2 / 2, \quad (2)$$

where m is the mass of one carbon atom.

Upon doping, electrons are transferred from the potassium to the carbon atoms. The doped system feels an additional electrostatic potential

$$U_1 = \frac{e^2}{4\pi\epsilon_0} \left[\frac{\lambda^2}{2(d+x)} - \frac{4\lambda}{r} \right], \quad (3)$$

where it was assumed that the potassium ions have the partial charge $+e$ and the carbon ions have the partial charge $-\lambda e$ with the elementary charge e and $0 < \lambda \ll 1$. For simplicity, we used a symmetric arrangement in our model. As long as $R \gg d$ the actual arrangement of the K⁺ ions plays only a minor role. Assuming that the K⁺ ions are mainly located in the center of the channels between the tubes in a bundle $R \approx 0.3$ nm (for a bundle of (10,10) tubes) has to be compared with $d = 0.07$ nm.

The carbon atoms are allowed to displace in the vertical direction (see Fig. 10) by the small amount x , thus

$$U_1 \approx \frac{e^2}{4\pi\epsilon_0} \left[\left(\frac{\lambda^2}{2d} - \frac{4\lambda}{R} \right) + \left(\frac{4\lambda d}{R^3} - \frac{\lambda^2}{2d^2} \right) x + \left(\frac{\lambda^2}{d^3} + \lambda \frac{4R^2 - 12d^2}{R^5} \right) \frac{x^2}{2} + \dots \right]. \quad (4)$$

For this expression we derive an equation of motion in the harmonic approximation:

$$\begin{aligned}
 m\ddot{x} + m\omega_0^2x + \frac{e^2}{4\pi\epsilon_0} \left(\lambda^2 + \lambda \frac{4R^2d^3 - 12d^5}{R^5} \right) \frac{x}{d^3} \\
 = \frac{e^2}{4\pi\epsilon_0} \left(\frac{\lambda^2}{2d^2} - \frac{4\lambda d}{R^3} \right). \quad (5)
 \end{aligned}$$

The constant force on the right-hand side results in an increased C-C equilibrium distance which in turn should cause a decrease of ω_0 . However, such a relationship was not included in our model. The last term on the left-hand side results in a frequency shift due to the additional Coulomb interactions. The new frequency will be

$$\begin{aligned}
 \omega &= \omega_0 \sqrt{1 + \frac{k}{\omega_0^2} \left(\lambda^2 + \lambda \frac{4R^2d^3 - 12d^5}{R^5} \right)} \\
 &\approx \omega_0 + \frac{k}{2\omega_0} \left(\lambda^2 + \lambda \frac{4R^2d^3 - 12d^5}{R^5} \right), \quad (6)
 \end{aligned}$$

where $k = e^2 / (4\pi\epsilon_0 m d^3) \approx 3.376 \times 10^{28} \text{ s}^{-2}$. Using $\omega_{[s^{-1}]} = 200\pi c_{[m/s]} \bar{\nu}_{[cm^{-1}]}$ and setting $\bar{\nu}_0 = 1590 \text{ cm}^{-1}$ we finally get

$$\bar{\nu} = (1590 + 299\lambda^2 + 13\lambda) \text{ cm}^{-1}. \quad (7)$$

This formula describes the position of the C-C ‘‘G line’’ and its upshift upon charge transfer as long as the decrease of ω_0 can be neglected (low doping levels). When the decrease in ω_0 gets larger, the ‘‘G line’’ shifts to lower frequencies. Within its limits, this simple model applies to the G-line shift due to *p*- and *n*-type doping of SWCNTs in general.

After doping step III, the average upshift of the outer tubes G line is 10 cm^{-1} . This would correspond to a charge transfer of about $0.16 e^-$ per carbon atom in our simple model, which is about a factor 5 too large. However, considering the simplicity of the model, the result is in good qualitative agreement.

When applying our simple model to the inner tubes we are assuming that the Coulomb interaction between the K ions outside the outer tube and the C ions of the inner tube can be neglected. However, the negatively charged C ions of the outer tube have now to be considered. For simplicity, we thus change in Fig. 10 the K^+ ions to C ions of the outer tube with partial charge $-\lambda_o e$. The two C ions on the C-C molecule represent now the inner tube and have a partial charge $-\lambda_i e$. Since the charge is at first transferred only to the outer tube, $0 < \lambda_i < \lambda_o \ll 1$. Additionally, R is now the radius difference between inner and outer tube, $R \approx 0.35 \text{ nm}$. With these changes Eq. (3) becomes

$$U_1 = \frac{e^2}{4\pi\epsilon_0} \left[\frac{\lambda_i^2}{2(d+x)} + \frac{4\lambda_o\lambda_i}{r} \right], \quad (8)$$

where the sign of the second term inside the brackets is the opposite as in Eq. (3). Hence, Eq. (6) becomes

$$\omega \approx \omega_0 + \frac{k}{2\omega_0} \left(\lambda_i^2 - \lambda_o\lambda_i \frac{4R^2d^3 - 12d^5}{R^5} \right) \quad (9)$$

and using $\bar{\nu}_0 = 1580 \text{ cm}^{-1}$ for the inner tube, we finally get

$$\bar{\nu} = (1580 + 301\lambda_i^2 - 8\lambda_o\lambda_i) \text{ cm}^{-1}. \quad (10)$$

The second term in the parentheses in Eq. (6) stems from the Coulomb attraction between the K and C ions and gives an additional contribution to the upshift of the G line. However, the second term in the parentheses in Eq. (9) is due to the Coulomb repulsion of the C ions on the outer and inner tube. This repulsion reduces the upshift of the G line. Certainly, this is a rather rough model. For a more accurate description of the inner tube behavior more C ions of the inner and outer tube should be considered. Nevertheless, even this simple model can in principle explain why there is an upshift for the outer tubes G line but a (smaller) downshift of the inner tubes G line.

Additionally, the constant force on the right hand side of Eq. (5) becomes

$$\frac{e^2}{4\pi\epsilon_0} \left(\frac{\lambda_i^2}{2d^2} + \frac{4\lambda_o\lambda_i d}{R^3} \right). \quad (11)$$

Thus, the increase in the C-C bond length for the inner tubes is relatively larger compared to the outer tubes which counteracts a frequency upshift. For both outer and inner tubes our model only describes the low doping regime where the increase of the force constants due to the Coulomb interaction dominates. This process competes with a decrease of the force constants due to the increase in C-C bond length not explicitly included in the frequency shift in our model. Upon further doping the latter effect dominates and the G band shifts to lower frequencies.

We now discuss the detailed investigation of the doping dependence of the cluster components of the (8,3) and (7,5) inner tubes RBM response as it was depicted in Figs. 8 and 9. First the intuitive notion that those inner tubes which have a smaller distance to their respective outer tubes are more easily affected by the doping can be investigated. We found that at the first doping step those peaks from the (8,3) cluster with a smaller distance between inner and outer tube (peaks 5–7) vanish quicker than those with a larger diameter difference (peaks 2–4) while on further doping the peak intensities decrease rather uniformly.

At the same time the doping behavior of the (8,3) cluster and the doping behavior of the (7,5) cluster are definitely different. This can already be seen from the absolute intensities in the right panel of Fig. 7: in the pristine sample the response of the (8,3) cluster is much stronger than that of the (7,5) cluster, after doping step I the intensity ratio is already slightly decreased while after doping step II the intensities of the two clusters are similar. Interestingly, after doping step III the intensity ratio of the (8,3) to the (7,5) cluster increased again. The same can be observed in the high-resolution spectra of the inner tube response upon 676 nm excitation: The intensity of nearly all of the peaks from the (8,3) cluster drops to more than half of its initial value at the first doping step while the intensities of the peaks from the (7,5) cluster even increase.

These results suggest that the doping of the inner tubes does not depend strongly on the diameter difference between the two shells or that a dependence on the diameter difference is outweighed by other effects like those discussed in the following.

In order to interpret the doping behavior we have to consider the mechanisms which induce the loss of Raman intensity. It is well established that Raman resonance is lost when the conduction band is filled high enough to fill the VHSs responsible for the resonance so that the according optical transition is no longer possible. However, the Fermi level has to be shifted by roughly half the excitation energy in order to fulfill this condition. At least at the very first doping level we do not expect this to be the case for the inner tubes. Another possibility is the smearing out of the VHS upon doping as it was observed in photoemission experiments.³¹ This effect is attributed to the influence of the K atoms which evoke a more three-dimensional behavior in the SWCNT bundles. This can explain the overall decrease in peak intensity upon increasing doping but cannot hold as an explanation for the qualitative difference in the doping behavior of the two inner tube clusters. A conceivable explanation for this could be that the transition energy between VHSs changes upon doping. From NTB calculations of the gap energy upon the removal of a certain amount of electrons it was claimed that *p*-type doping leads to a change in the VHS transition energy of SWCNT.³⁷ For family 19 a noticeable upshift of the E_{22}^S transition energy was calculated for the removal of 0.04 electrons per carbon atom, which is a relatively high doping level. However, since the mechanism of this effect remains unclear, the direction of the gap energy change in a similar calculation for *n*-type doping is unknown. The results at hand—an overall decrease of intensity of the (8,3) cluster accompanied with a slight increase of intensity of the (7,5) cluster at the first doping step—could be explained with a decrease in the E_{22}^S transition energy of these tubes.

Additionally, for the discussed diameter difference ranges all three types of SWCNTs, namely metallic (M) as well as semiconducting type I (SI) and type II (SII) tubes, act as outer tubes for the (7,5) and (8,3) inner tubes. Since the latter are of type SI the following inner/outer tube pairs contributed to the 676 nm spectra: SI/M, SI/SI, and SI/SII. For all these combinations a similar doping behavior was observed.

This is in agreement with *p*-type doping experiments³⁷ where the authors report that S/S and S/M configurations behave similarly upon Br₂ adsorption on DWCNTs and with the modeling of bromine-doped DWCNTs as three-layer cylindrical capacitors.²²

V. CONCLUSION

In summary, we presented a detailed Raman study of the *n*-type doping of DWCNTs. We investigated the doping behavior of the two main Raman features, the G line and the radial breathing mode. In both cases the response from the outer tubes decreased faster upon doping than that for the inner tubes, which shows that the charge is first transferred to the outer tube. Additionally, the G line of the outer tubes hardens while that of the inner tubes softens during the doping process. Both shifts were explained by additional Coulomb forces in the different electronic environments of the inner and outer tubes. For even heavier doping than discussed here, the G lines of inner and outer tubes soften which can be explained by an expansion of the C-C bonds similar to observations in GICs.

The clustered high-resolution inner tube RBM response was attributed to different inner tube–outer tube configurations. An analysis of the changes of the relative peak intensities as a function of diameter difference between inner and outer tubes revealed a nonuniform behavior for the two cases indicating the existence of a complex doping dependence where the diameter difference is not the only factor that influences charge transfer to the inner tubes.

ACKNOWLEDGMENTS

This work was supported by the DFG. R.P. acknowledges support from FWF project P17345. F.S. was supported by EU project MERG-CT-2005-022103, the Hungarian State Grants No. TS049881, F61733, and NK60984 and the Zoltán Magyary programme. V.N.P. was supported by Marie-Curie project MEIF-CT-2003-501080.

*Present address: Budapest University of Technology and Economics, Institute of Physics and Solids in Magnetic Fields, Research Group of the Hungarian Academy of Sciences, H-1521, Budapest, P.O. Box 91, Hungary.

¹B. W. Smith, M. Monthieux, and D. E. Luzzi, *Chem. Phys. Lett.* **315**, 31 (1999).

²S. Bandow, M. Takizawa, K. Hirahara, M. Yudasaka, and S. Iijima, *Chem. Phys. Lett.* **337**, 48 (2001).

³R. Pfeiffer, H. Kuzmany, C. Kramberger, C. Schaman, T. Pichler, H. Kataura, Y. Achiba, J. Kürti, and V. Zólyomi, *Phys. Rev. Lett.* **90**, 225501 (2003).

⁴A. M. Rao, P. C. Eklund, S. Bandow, A. Thess, and R. E. Smalley, *Nature (London)* **388**, 257 (1997).

⁵T. Pichler, H. Kuzmany, H. Kataura, and Y. Achiba, *Phys. Rev. Lett.* **87**, 267401 (2001).

⁶F. Wang, G. Dukovic, L. E. Brus, and T. F. Heinz, *Science* **308**, 838 (2005).

⁷V. N. Popov, *New J. Phys.* **6**, 17 (2004).

⁸G. G. Samsonidze, R. Saito, N. Kobayashi, A. Gruneis, J. Jiang, A. Jorio, S. G. Chou, G. Dresselhaus, and M. S. Dresselhaus, *Appl. Phys. Lett.* **85**, 5703 (2004).

⁹R. Pfeiffer, F. Simon, H. Kuzmany, and V. N. Popov, *Phys. Rev. B* **72**, 161404(R) (2005).

¹⁰X. Liu, T. Pichler, M. Knupfer, and J. Fink, *Phys. Rev. B* **67**, 125403 (2003).

¹¹F. Simon, Á. Kukovecz, C. Kramberger, R. Pfeiffer, F. Hasi, H. Kuzmany, and H. Kataura, *Phys. Rev. B* **71**, 165439 (2005).

¹²H. Kataura, Y. Maniwa, T. Kodama, K. Kikuchi, K. Hirahara, K. Suenaga, S. Iijima, S. Suzuki, Y. Achiba, and W. Krätschmer, *Synth. Met.* **121**, 1195 (2001).

¹³H. Kataura, Y. Kumazawa, Y. Maniwa, I. Umezumi, S. Suzuki, Y. Ohtsuka, and Y. Achiba, *Synth. Met.* **103**, 2555 (1999).

¹⁴V. N. Popov and P. Lambin, *Phys. Rev. B* **73**, 165425 (2006).

¹⁵G. Bussi, J. Menendez, J. Ren, M. Canonico, and E. Molinari,

- Phys. Rev. B **71**, 041404(R) (2005).
- ¹⁶J. Jiang, R. Saito, A. Gruneis, S. G. Chou, Ge. G. Samsonidze, A. Jorio, G. Dresselhaus, and M. S. Dresselhaus, Phys. Rev. B **71**, 205420 (2005).
- ¹⁷A. Jorio, G. Dresselhaus, M. S. Dresselhaus, M. Souza, M. S. S. Dantas, M. A. Pimenta, A. M. Rao, R. Saito, C. Liu, and H. M. Cheng, Phys. Rev. Lett. **85**, 2617 (2000).
- ¹⁸O. Dubay, G. Kresse, and H. Kuzmany, Phys. Rev. Lett. **88**, 235506 (2002).
- ¹⁹V. N. Popov and P. Lambin, Phys. Rev. B **73**, 085407 (2006).
- ²⁰F. Simon, C. Kramberger, R. Pfeiffer, H. Kuzmany, V. Zólyomi, J. Kürti, P. M. Singer, and H. Alloul, Phys. Rev. Lett. **95**, 017401 (2005).
- ²¹S. Bandow, G. Chen, G. U. Sumanasekera, R. Gupta, M. Yudasaka, S. Iijima, and P. C. Eklund, Phys. Rev. B **66**, 075416 (2002).
- ²²G. Chen, S. Bandow, E. R. Margine, C. Nisoli, A. N. Kolmogorov, V. H. Crespi, R. Gupta, G. U. Sumanasekera, S. Iijima, and P. C. Eklund, Phys. Rev. Lett. **90**, 257403 (2003).
- ²³R. Pfeiffer *et al.* (unpublished).
- ²⁴R. S. Lee, H. J. Kim, J. E. Fischer, A. Thess, and R. E. Smalley, Nature (London) **388**, 255 (1997).
- ²⁵N. Bendiab, L. Spina, A. Zahab, P. Poncharal, C. Marlière, J. L. Bantignies, E. Anglaret, and J. L. Sauvajol, Phys. Rev. B **63**, 153407 (2001).
- ²⁶L. Grigorian, G. U. Sumanasekera, A. L. Loper, S. Fang, J. L. Allen, and P. C. Eklund, Phys. Rev. B **58**, R4195 (1998).
- ²⁷G. T. Kim, E. S. Choi, D. C. Kim, D. S. Suh, Y. W. Park, K. Liu, G. Duesberg, and S. Roth, Phys. Rev. B **58**, 16064 (1998).
- ²⁸J. E. Fischer, H. Dai, A. Thess, R. Lee, N. M. Hanjani, D. L. Dehaas, and R. E. Smalley, Phys. Rev. B **55**, R4921 (1997).
- ²⁹G. U. Sumanasekera, J. L. Allen, S. L. Fang, A. L. Loper, A. M. Rao, and P. C. Eklund, J. Phys. Chem. B **103**, 4292 (1999).
- ³⁰G. Chen, C. A. Furtado, S. Bandow, S. Iijima, and P. C. Eklund, Phys. Rev. B **71**, 045408 (2005).
- ³¹H. Rauf, T. Pichler, M. Knupfer, J. Fink, and H. Kataura, Phys. Rev. Lett. **93**, 096805 (2004).
- ³²T. Pichler, A. Kukovecz, H. Kuzmany, H. Kataura, and Y. Achiba, Phys. Rev. B **67**, 125416 (2003).
- ³³H. Rauf, H. Shiozawa, T. Pichler, M. Knupfer, B. Büchner, and H. Kataura, Phys. Rev. B **72**, 245411 (2005).
- ³⁴H. Rauf, T. Pichler, F. Simon, and H. Kuzmany, in *Proceedings of the XVIII International Winterschool/Euroconference on Electronic Properties of Novel Materials*, edited by H. Kuzmany, J. Fink, M. Mehring, and S. Roth (2004), pp. 213–216.
- ³⁵M. S. Dresselhaus and G. Dresselhaus, Adv. Phys. **30**, 139 (1981).
- ³⁶J. Cambedouzou, J.-L. Sauvajol, A. Rahmani, E. Flahaut, A. Peigney, and C. Laurent, Phys. Rev. B **69**, 235422 (2004).
- ³⁷A. G. Souza Filho, M. Endo, H. Muramatsu, T. Hayashi, Y. A. Kim, E. B. Barros, N. Akuzawa, Ge. G. Samsonidze, R. Saito, and M. S. Dresselhaus, Phys. Rev. B **73**, 235413 (2006).